First publ. in: Journal of Catalysis 241 (2006), 2, pp. 446-455

Cu/ZnO aggregates in siliceous mesoporous matrices: Development of a new model methanol synthesis catalyst

M.W.E. van den Berg [a], S. Polarz [b,*], O.P. Tkachenko [a,1], K.V. Klementiev [a,d], M. Bandyopadhyay [c], L. Khodeir [a], H. Gies [c], M. Muhler [a], W. Grünert [a,*]

[a] *Lehrstuhl für Technische Chemie, Ruhr-Universität Bochum, P.O. Box 102148, D-44780 Bochum, Germany*
[b] *Institute of Chemistry, Technical University Berlin, Berlin, Germany*
[c] *Lehrstuhl für Kristallographie, Ruhr-Universität Bochum, Bochum, Germany*
[d] *Hasylab, Hamburg, Germany*

Dedicated to Prof. Volker Staemmler at the occasion of his 65th birthday

Abstract

Copper and zinc were introduced into mesoporous siliceous matrices with the goal of obtaining model methanol synthesis catalysts with intense interaction between copper and the ZnO promoter. The preparation methods included various aqueous routes starting from acetate solutions (into MCM-48) and a route involving an organometallic step—thermolysis of a liquid heterocubane of Zn_4O_4 type ($[CH_3ZnOCH_2CH_2OCH_3]_4$) in a wormhole-type silica of 5 nm average pore size—followed by aqueous Cu (nitrate) impregnation. The materials were characterized by XRD, nitrogen physisorption, N_2O frontal chromatography, TPR, and EXAFS, and their methanol synthesis activity was measured at 493 K and normal pressure. In the aqueous preparations with acetate solutions, excessive formation of silicates (particularly zinc silicate) led to damage of the pore system. A significant delay in Cu reduction was assigned to the influence of micropores formed, together with some copper silicate formation. These samples exhibited poorly accessible Cu surface areas despite small Cu particle sizes indicated by EXAFS and disappointing methanol synthesis activity. In contrast to this, a highly active catalyst was obtained via the heterocubane route that meets industrial standards in terms of reaction rate per Cu surface area. Orientation studies (EXAFS at the Cu*K* and Zn*K* edges) reflecting a redox behavior of the ZnO_x component illustrate the potential of this catalyst type for use in basic studies of the Cu–ZnO_x interaction in methanol synthesis catalysts.

Keywords: Methanol synthesis; Copper; Zinc oxide; Metal–support interaction; Model catalyst; Mesoporous silica; MCM-48; XAFS; TPR

1. Introduction

Today it is widely accepted that in the Cu/ZnO/Al_2O_3 methanol synthesis catalyst, the interaction between Cu and ZnO plays a vital role in the development of high catalytic activity. The mechanism of this interaction remains under discussion. The most relevant models agree in assuming that defective ZnO created in a strongly reductive atmosphere exerts a dramatic influence on the copper, but they differ in the interpretation of the consequences on the active copper site, which is considered a metallic site by most, but not all, groups.

It has been found that the defective ZnO causes changes in the particle morphology of the copper (wetting/nonwetting effect) [1–3], which leads to different exposures of copper facets, particularly of the most active (111) facet. Based on this finding, attempts have been made to fit real kinetic data of methanol synthesis with a microkinetic model, in which kinetic data for the steps of the underlying reaction mechanism are taken from stud-

* Corresponding authors. Fax: +49 234 321 4115.
E-mail addresses: sebastian.polarz@tu-berlin.de (S. Polarz), w.gruenert@techem.rub.de (W. Grünert).
[1] On leave from: N.D. Zelinsky Institute of Organic Chemistry, Russian Academy of Sciences, Moscow, Russia.

ies on Cu single-crystal surfaces. The fact that this model has been successful when complemented with a routine describing the exposure of these surfaces with varying oxidation potentials of the mixture [4] suggests that the morphology change alone explains the promoting influence of the zinc.

An alternative view has been advocated by Günter et al., according to which the intrinsic activity of copper is enhanced by strain imposed on it by the interaction with ZnO (misfit at the contact surface, bulk inclusion of ZnO_x entities [5,6]). This mode of activation, which might be a general feature of metal–support relations, was observed for methanol synthesis and methanol steam reforming.

It is, however, also known that under strongly reducing conditions, ZnO_x species migrate onto the copper surface [2,7,8], which has a favorable effect on methanol synthesis activity. This suggests that sites of particular reactivity may exist at the Cu–ZnO_x interface, the extension of which increases when ZnO_x species migrate onto the Cu surface. This view has been supported by groups that adhere to Cu metal as the active site for methanol synthesis [2,8,9], as well as by those that advocate a deciding role for Cu^+ [10–13]. However, with a traditional $Cu/ZnO/Al_2O_3$ catalyst, the comparison of TPD experiments (H_2 TPD vs. N_2O titration) after methanol synthesis and after CO treatment implies that the actual coverage of the Cu surface by ZnO_x may be quite low under actual reaction conditions [8]. But because a moderately active Cu/Al_2O_3 catalyst can be dramatically boosted by gas-phase interaction with diethyl zinc [9], it has been concluded that the Cu–ZnO interface plays a vital role in methanol synthesis.

There are several reasons why obtaining reliable insight into the nature of the Cu–ZnO interaction from experiments with catalysts of technical interest is very difficult. Although prepared by seemingly simple methods (co-precipitation, calcinations), the actual microstructures of the catalyst precursors and the resulting catalytic materials after activation are very complex and depend on many parameters that are difficult to control. In addition, studying the interface between Cu particles and ZnO aggregates is very complicated, because at particle sizes of several nm (and well above 10 nm for ZnO), only a very small percentage of the Cu atoms (or Zn ions) are engaged in the mutual interaction. This percentage can be increased by imposing a high dispersion on *both* Cu and ZnO, which should be beneficial to the catalyst's general performance as well [9].

The approach adopted by our groups to force the catalyst components into high dispersion and intense interaction with one another simultaneously provides an opportunity to apply more well-defined preparation steps. By embedding the catalytically active component into a well-defined superstructure (e.g., a hierarchically structured mesoporous matrix), it should be possible to simultaneously simplify and miniaturize the supported catalyst [14–20] and to utilize in the preparation the favorable effects of the spatially confined reaction conditions on the chemistry occurring in the porous solid [21]. However, this approach carries the risk of interference by the pore walls of the matrix. Indeed, a strong interaction was previously observed between the silicate wall and zinc species introduced by aqueous techniques or by interaction with dimethyl zinc, which was stable during calcination and rendered the zinc in a completely disordered state, probably as a zinc silicate layer covering the wall instead of nanoparticulate ZnO [22,23]. In redox experiments in which the response of the IR reflectivity on changes in the gas atmosphere was followed, these zinc species turned out to be redox-inactive [23], unlike bulk ZnO.

The activation of copper particles previously produced in the mesoporous matrix by treatment with diethyl zinc seems an obvious approach for the creation of a large Cu–ZnO_x interface, and it has been realized in a companion work in which copper was introduced from a volatile organometallic source as well [24]. But although this preparation demonstrates that active methanol synthesis catalysts can be obtained by the miniaturization approach described above, most of the zinc ends up deactivated at the pore walls in this case as well, impeding the goal of studying those zinc species engaged in the Cu–ZnO interaction.

The goal of our research was to create a matrix-encapsulated methanol synthesis catalyst that combines high activity with high potential for investigation of the metal–support interaction. After considerable effort aimed at achieving this goal with seemingly simple preparations starting from aqueous copper and zinc acetate solutions [22,23], a promising catalyst was obtained via a route involving the deposition of zinc into a mesoporous silicate via thermolysis of a liquid organometallic precursor [16]. Conventional impregnation of such ZnO-modified mesoporous silicate with copper nitrate resulted in a methanol synthesis catalyst with an activity of the same order of magnitude as a catalyst of technical relevance and clear indications of zinc redox activity as demonstrated by XAFS. In this paper, structural and catalytic data for the new model catalyst are compared with results from a typical material obtained via the aqueous route to illustrate the critical points in the synthesis. We show that the new material, which is a simplified but competitive catalyst obtained via a complicated route, opens up an interesting approach for both further optimization and model studies on the nature of the Cu–ZnO interaction.

2. Experimental

2.1. Materials

The matrix used in the present study is a mesoporous silica with a wormhole-type pore structure. The preparation of silica monoliths with tunable mesopore size via the true liquid-crystal templating route has been described elsewhere [16,25,26]. These materials have a bicontinuous pore system, with micropores connecting the mesopores. In this study, we concentrate on a material with an average pore size of 50 Å prepared with Pluronic P123 as a template, labeled as wh(50)-SiO_2. For comparison, a preparation with an MCM-48 matrix is reported as well. The synthesis of this matrix has been described previously [23] where characterization data are given as well [XRD—*d* spacing of (211) reflection—3.272 nm].

The organometallic precursor of "Zn_4O_4" heterocubane type ($[CH_3ZnOCH_2CH_2OCH_3]_4$ (**I**)),

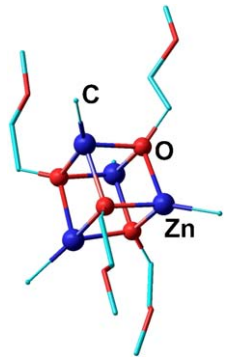

I

which contains the ZnO in preformed nanounits, is a liquid. This permits its introduction into pore systems at very different loadings. The detailed procedure for the preparation of size-selected, nanocrystalline ZnO particles has been reported elsewhere [27]. In brief, the porous matrix was loaded by liquid infiltration with (**I**) or with its solution in *n*-pentane, the concentration of which was chosen to achieve the desired Zn content. Subsequent thermolysis of the precursor in synthetic dry air at 523 K (at a temperature ramp of 5 K/min) led to formation of ZnO. Copper was introduced via the traditional impregnation route using a saturated copper nitrate solution or dilutions. After infiltration for at least 24 h, the samples were dried in a rotary-pump vacuum for 3 days.

From the several aqueous routes tried in an attempt to encapsulate the methanol synthesis catalyst into siliceous MCM-48 (e.g., coimpregnation of acetates, impregnation of copper into a MCM-48 previously reacted with diethyl zinc, intraporous urea precipitation of acetates), we chose for presentation in this paper a material obtained by a synthesis aiming at an intraporous carbonate precipitation akin to that used for the technical catalyst. For this purpose, Cu and Zn acetates were simultaneously deposited into MCM-48 by dry (co)impregnation from saturated acetate solution and subsequent freeze-drying. The pores were then filled with a 1 M Na_2CO_3 solution to precipitate the dissolving copper and zinc acetate deposits as carbonate. Subsequently, the sample was dried at room temperature and calcined at 573 K for 8 h after heating at a 1 K/min temperature ramp.

For comparison, a monometallic Cu-MCM-48 sample is included in this presentation. Its preparation (via impregnation of MCM-48 with copper acetate solution) and structural properties have been described previously [28].

Table 1 summarizes the samples and gives their metal content and the labels used to describe them throughout this paper. The compositions were determined by ICP analysis or assessments on the basis of the XAFS step heights, which have given comparable results over a wide range of materials studied [22,23].

2.2. Methods

Temperature-programmed reduction (TPR) was carried out with a mixture containing 4.2 vol% H_2 in Ar (84 ml/min), ramping the temperature at 10 K/min from room temperature to 800 °C. The hydrogen content of the effluent was measured by a catharometry-based instrument (Hydros, Fisher-Rosemount). Where possible, the criteria derived by Monti and Baiker [29] for optimum conditions of the experiment were obeyed. Where this was not possible due to low amounts of available sample, a drift of the baseline was superimposed on the (weak) H_2 consumption signal (Fig. 2); this does not affect the conclusions drawn from the data, however. The hydrogen consumption corresponded to the complete reduction of Cu(II) to metallic copper within the limits of experimental error (which were, however, substantial in runs with small amounts of catalyst).

XAFS spectra (Cu*K* edge, 8.979 keV; Zn*K* edge, 9.659 keV) were measured in transmission mode at Hasylab E4 station (Hamburg). A Si(111) double-crystal monochromator was used, which was detuned to 50% of maximum intensity to exclude higher harmonics from the X-ray beam. The self-supported pressed samples were reduced in an in situ EXAFS cell [30] in a flow of 5% H_2/He at a temperature ramp of 5 K/min and a 15-min isothermal period at the reduction temperature. The spectra (absorption μ) were then taken at liquid nitrogen temperature, and the spectrum of a Cu (or Zn) foil was recorded at the same time (between the second and third ionization chambers) for energy calibration. In the subsequent run, the previous reduction temperature was established with a 10 K/min ramp, and the next temperature was approached with 5 K/min.

The data were processed using the VIPER software package [31]. For background subtraction, a Victoreen polynomial was fitted to the pre-edge region. The smooth atomic background, μ_0, was estimated using a smoothing cubic spline. The Fourier analysis of the k^2-weighted experimental function $\chi = (\mu - \mu_0)/\mu_0$ was performed with a Kaiser window. Theoretical references calculated by the FEFF8.10 code [32] were used for the determination of structural parameters. To minimize the number of free parameters, equal backscatters were fitted with the same E_0-shift wherever possible.

The influence of the Cu EXAFS on the nearby Zn spectrum was tested with a sample of high Cu content [aqueous coimpregnation; data not shown here due to similarities with those of CuZn-MCM(carb)] after reduction of the copper to the metal-

Table 1
Preparation procedures and compositions of samples used in the present study

Sample code	Matrix	Preparation[a]	wt% Cu//Zn (*ICP*, **XAFS**)
Cu-MCM	MCM-48	Impregnation	*5.6*
CuZn-MCM(carb)	MCM-48	Intraporous carbonate precipitation	*3.8* (**4.6**)//**9.5**
om-CuZn–M(I)	wh(50)-SiO_2	Heterocubane route, see text	**9.9//16.6**
om-CuZn–M(II)	wh(50)-SiO_2	Heterocubane route, see text	**9.9//4.0**

[a] See Section 2.

lic state. For this test, the model parameters for the Cu particles were extracted from the CuK spectrum, which was then simulated in full length (i.e., extending over the ZnK edge) with these data and subtracted from the ZnK XAFS. The comparison between uncorrected and corrected Zn EXAFS show a negligible influence of copper on the zinc spectrum.

X-ray diffractograms were recorded with a Bruker-AXS D8 Advance instrument using CuK_α radiation ($\lambda = 1.5418$ Å) and a position-sensitive detector (PSD) in the 2θ range from 25° to 85° with 0.015° steps.

2.3. Catalysis

The activity measurements were carried out in a fixed-bed glass-lined U-tube reactor. Samples of 100 mg (sieve fraction, 250–355 μm) were reduced in flowing diluted H_2 (2% H_2 in He) at 473 K for 16 h. To ensure complete reduction, the temperature was increased to 493 K and the sample treated with pure H_2. For samples based on the MCM-48 matrix, in which higher temperatures are required for the reduction of Cu, the final reduction temperature was increased up to 353 K (in pure H_2). The active surface area of copper was determined by N_2O reactive frontal chromatography at room temperature [33]. Methanol activity was measured at atmospheric pressure and 493 K. The synthesis gas was composed of 72% H_2, 10% CO, 4% CO_2, and 14% He. Gases of highest purity (>99.9995%) were used. Analysis of the gas phase was performed using a calibrated quadrupole mass spectrometer (Balzers GAM 422).

For comparison, activity data were also measured for a Cu/ZnO/Al_2O_3 catalyst of industrial interest (ca. 50% Cu, 35% ZnO, and 15% Al_2O_3).

3. Results and discussion

3.1. Characterization of samples prior to reduction

Powder XRD patterns measured after the introduction of zinc and/or copper into wh(50)-SiO_2 are shown in Fig. 1. Traces a and b were taken after introduction of copper (via aqueous copper nitrate solution) and zinc [via (**I**); see Section 2] alone; trace c shows the situation after sequential impregnation, with an excess of Cu over Zn (10% Cu, 4% Zn). The reflections can be completely assigned to $Cu(NO_2)_6(OH)_6$ in trace (a) and to ZnO in trace (b), with particle sizes of 4.6 and 3.9 nm, respectively, derived from the line widths via Scherrer's equation. After sequential impregnation (c), a coexistence of both phases apparently occurred, consisting of very small particles. The different scattering intensities assigned to the different phases are in good agreement with an excess of the Cu^{2+} salt. Interestingly, according to a refined analysis of the PXRD data (Warren-Averbach), the $Cu(NO_2)_6(OH)_6$ particles were somewhat smaller ($d_{\text{particle}} \approx 3$ nm) after the sequential impregnation. However, it seems that the porous environment successfully confined the growth of both ZnO and $Cu(NO_2)_6(OH)_6$, and these phases likely were intimately mixed on the nanoscale.

Both the choice of the ZnO precursor and the pore size are important parameters for obtaining a suitable catalyst. This is

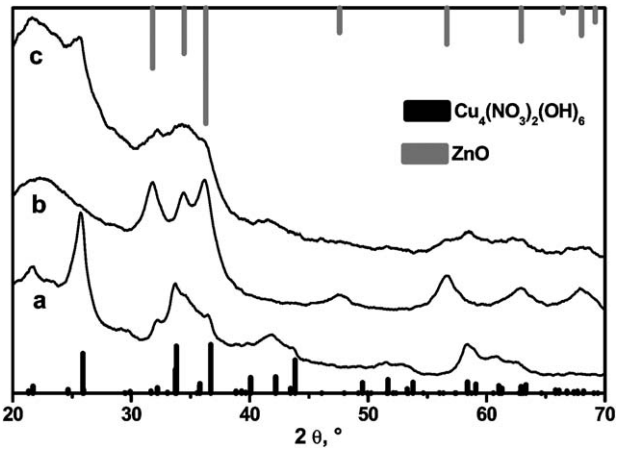

Fig. 1. X-ray diffractograms of Cu and Zn species introduced into wh(50)-SiO_2. (a) Impregnation with aqueous $Cu(NO_3)_2$ solution, (b) intraporous thermolysis of heterocubane (**I**) at 523 K in dry air, (c) thermolysis of (**I**) followed by impregnation with aqueous $Cu(NO_3)_2$ solution, approximate composition—10% Cu, 4% Zn.

documented by our experiments on MCM-48 and the introduction of Cu and Zn by aqueous methods (see Section 2). Here, according to powder XRD, no crystalline phases appeared. Furthermore, the introduction of the metal species led to a strong reduction of the low-angle XRD indicative of the meso-character of the porous matrix. The latter effect can be caused by either lattice destruction or successful introduction of heavy elements into the pore system (decreased scattering contrast [22]). Lattice destruction is a problem, however, particularly when Zn acetate is involved [23], although the extent of the damage appears to depend on conditions that are not entirely clear. In the case of CuZn-MCM(carb), a BET surface area of just 180 m^2/g (initial MCM-48—ca. 1260 m^2/g) was measured, with a wide pore size distribution between the micropores and macropores not related to the distribution in the parent MCM-48 (see supporting material).

3.2. Reduction studies

The formation of copper under confinement of the porous matrices was investigated by TPR and in situ XAFS. Fig. 2 presents TPR profiles of catalysts investigated in this study (normalized to the Cu content) and compares them with the TPR profile of CuO, which is reduced in a single sharp step at ca. 470 K. The reduction profile becomes broader when copper is introduced into the mesopores of MCM-48, but ≈80% of the hydrogen consumption still occurs in a single reduction peak at around 500 K. The profile of CuZn-MCM(carb) is typical of samples obtained by introduction of Cu and Zn acetates into MCM-48. The reduction begins in the same temperature range as in Cu–M or CuO, but the profiles are extremely wide and indicate hydrogen consumption well above 800 K. In contrast, the copper in om-CuZn–M(I) is reduced in a single step below 500 K. The profile resembles that of the monometallic Cu–M except for a weak tailing to higher temperatures instead of a separate high-temperature peak.

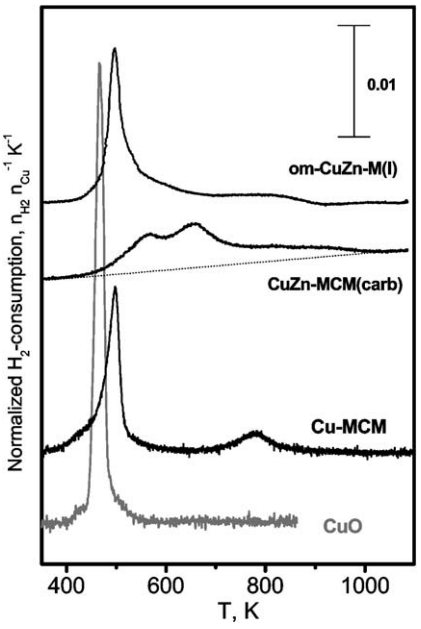

Fig. 2. Influence of zinc on the TPR profiles of Cu oxide species in mesoporous siliceous matrices.

Typical sets of Cu*K* XAFS spectra measured during the reduction of copper species in mesoporous siliceous matrices loaded both with CuO_x and ZnO_x are shown in Fig. 3 ((b), XANES region; (a) and (c), absolute value of k^2-weighted FT). As may be anticipated from the TPR profiles, the course of the reduction differs greatly between CuZn-MCM(carb) (which behaves similar to other preparations involving aqueous media in the introduction of zinc) and om-CuZn–M(I). In the XANES of CuZn-MCM(carb) (Fig. 3b), the formation of Cu(I) species is clearly apparent at around 550 K, whereas the typical shape of Cu(0) appears only at 595 K. In the EXAFS (Fig. 3c), Cu ions can be clearly seen to coexist with Cu(0) at 565 K and even 595 K (a shoulder at the main scattering signal). On the other hand, for the heterocubane-based om-CuZn–M(I), the development of the XANES during reduction suggests that the Cu(II) species in this material are directly converted to Cu(0) at low temperatures. In the EXAFS spectra of the Cu(0) species, the features between 3 and 5 Å, uncorrected, are somewhat blurred.

The first shell of the Cu*K* EXAFS spectra was fitted according to principles outlined previously [28] (see supporting material for detailed results). These results support the observation from XANES (Fig. 3b) that the reduction of Cu(II) oxide species in CuZn-MCM(carb) proceeds largely via the intermediate Cu(I) stage; the Cu–O distance shifts from 1.95 Å (initial sample) to 1.86 Å (565–595 K) before the oxide shell disappears. In the fully reduced state, which is achieved only at 695 K with this material, the fits yield a Cu(0)–Cu coordination number (CN) of 10.4. According to a geometrical correlation between first-shell CN and the diameter of (spherical) particles [34], this corresponds to particles of ca. 3 nm diameter. Similar results have been obtained with other Cu–Zn-MCM-48 materials prepared starting from metal acetates [35]. During reduction, extensive Cu(I) was observed on both XANES and EXAFS, and the Cu particle size achieved on full reduction was 2–3 nm, readily measurable by EXAFS.

In contrast, in om-CuZn–M(I), the Cu–O shell remained at the distance typical of Cu(II) (1.95–1.96 Å). At 535 K, Cu(0) appeared [Cu(0) CN 9.0], with only a minor contribution of residual Cu–O. After 15 min of reduction at 695 K, the Cu(0)–Cu CN increased slightly to 10.3; that is, the particles were of the same size as in CuZn-MCM(carb). In the monometallic Cu-MCM, the particles remained significantly smaller on reduction

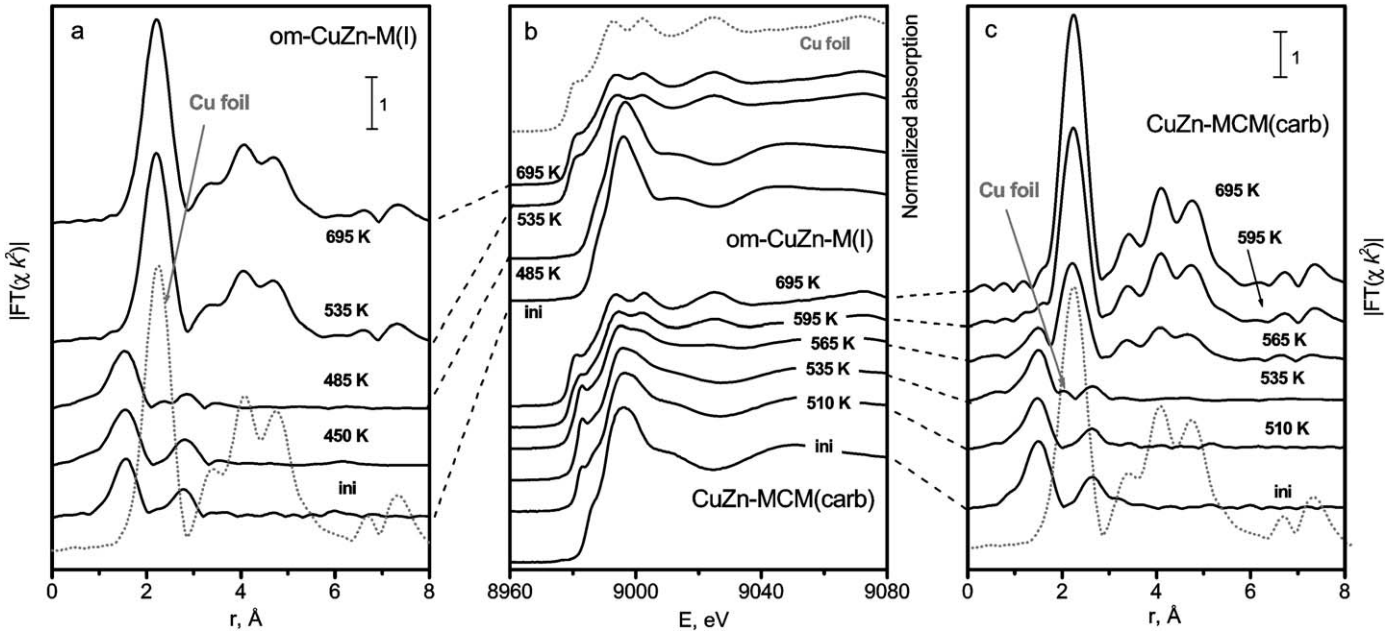

Fig. 3. Cu*K* XAFS spectra measured after reduction of om-CuZn–M(I) and CuZn-MCM(carb) at different temperatures indicated in the figure. (a) and (c) EXAFS, (b) XANES, all spectra measured at liquid nitrogen temperature. Cu(0)–Cu coordinations numbers for the highest reduction temperature (695 K) evaluated to 10.4 (CuZn-MCM(carb)) and 10.3 (om-CuZn–M(I)). For full set of data—see supporting material.

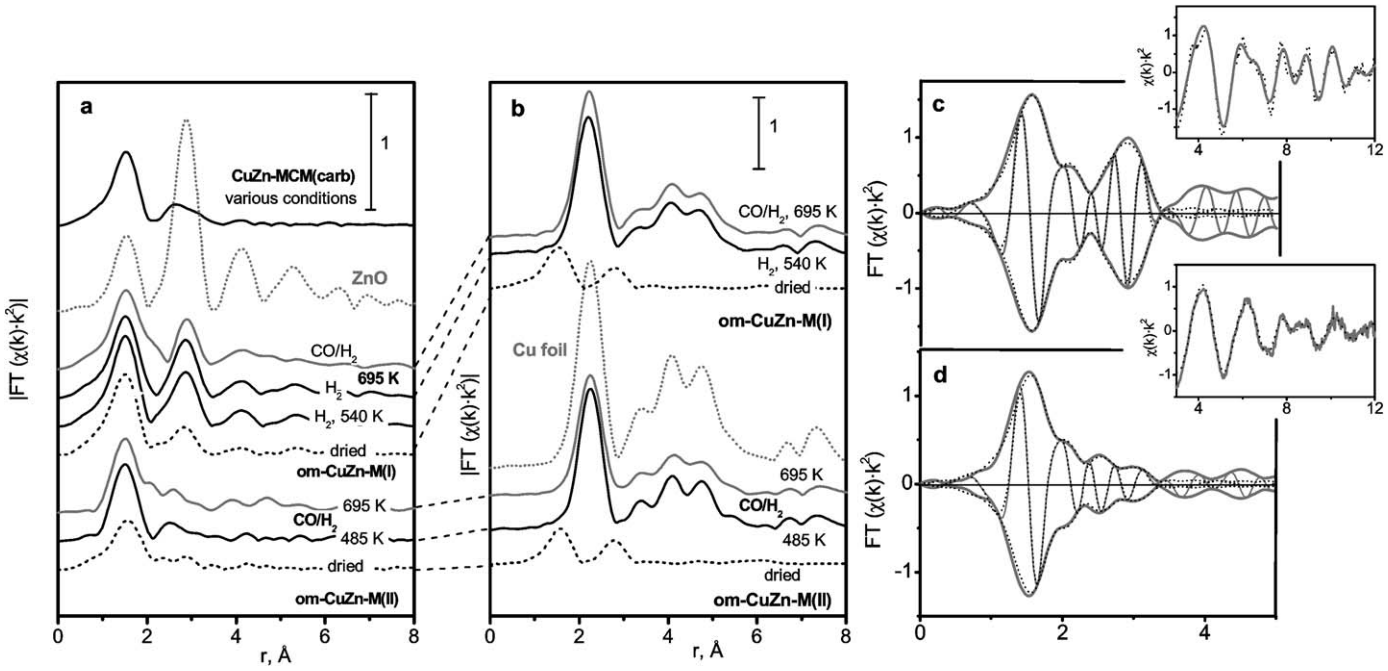

Fig. 4. Comparison of Zn*K* and Cu*K* XAFS spectra measured after reduction of copper in matrix-encapsulated CuO/ZnO preparations at different temperatures. (a) Zn*K* EXAFS, (b) Cu*K* EXAFS, (c) and (d) examples for fitting results for the spectra of (c) om-CuZn–M(I) and (d) om-CuZn–M(II), both after reduction in CO/H_2 at 695 K (15 min), models with Cu metal atom as second shell (cf. Table 3). Labels "H_2" and "CO/H_2" mean 5% H_2 in He, and 10% CO/H_2, respectively. All spectra measured at liquid nitrogen temperature.

[28], with Cu(0)–Cu CNs increasing from 8 to 9.5 between 500 and 770 K (particle size, 1.2–1.8 nm).

Zn*K* EXAFS spectra measured during these reduction runs are presented in Fig. 4a. The spectrum of CuZn-MCM(carb) is nearly invariable over the whole temperature range and clearly differs from that of ZnO; the second shell (Zn–Zn in ZnO) is not only much smaller in the matrix-encapsulated sample, but it apparently consists of two contributions at different distances than in the oxide. Hence, the Zn phase formed in this sample is different from ZnO. In the heterocubane-derived om-CuZn–M(I), a weak scattering feature appears at the distance expected for ZnO already in the initial state, pointing to the particulate nature of the zinc oxide species. On reduction of the copper (see also Fig. 3a), this second sphere grew somewhat, probably due to better ordering or particle growth on collection of the Cu oxide species into particles. However, as long as CO is absent from the reaction atmosphere, only minor changes in the Zn*K* EXAFS occur with further temperature increases.

The results presented so far reveal that different routes for introducing Cu and Zn into siliceous matrices have led to materials with extremely different reduction behaviors, although the final Cu species appears to be similar on the basis of EXAFS data. It is known that at the Cu contents discussed herein, copper alone reduces in a single step in MCM-48 [28]; see also Fig. 2. Two-step reduction schemes have been seen with other wet-prepared CuZn-MCM-48 samples as well, but not when the zinc was introduced via reaction of the matrix with diethylzinc [35]. Thus, we believe that lattice destruction due to silicate formation (mostly with zinc) is the origin of these phenomena. Lattice destruction by silicate formation has been recently observed during the preparation of Co-ZSM-5 from Co acetate (solid-state and liquid-exchange routes) [36]. Regarding copper and zinc, the interaction of the latter with the pore walls is much stronger than that of the former; Cu was found to form oxide nanoparticles in siliceous matrices, whereas zinc did not under comparable conditions [23].

Copper silicate formation was directly indicated by TPR (Fig. 2). With Cu-MCM, the high-temperature peak probably arose from such a phase; amorphous Cu-containing particles were seen in the TEM, but due to their high Cu content, they more likely were formed from an amorphous minority phase in the MCM-48 material [28]. The high-temperature shoulders in the TPR of ZnCu-MCM(carb) and om-CuZn–M(I) may be assigned to copper silicates as well. However, the splitting of the low-temperature peak in Cu–Zn-MCM(carb) cannot be ascribed to the same cause, because the maximum of the additional signal occurred at a rather low temperature (ca. 670 K). A similar splitting of the main reduction peak into two was found earlier for microporous matrices (silicalite-1, dealuminated Y), where intermediate Cu(I) was well detected by XAFS and high-temperature TPR peaks assignable to Cu silicates were completely absent [28]. Thus, we believe that the two-step reduction scheme found for ZnCu-MCM(carb) (and other wet-prepared samples) is due not so much to an interaction between Zn and Cu, but rather to perturbation of the pore system by the interaction of Zn with the pore walls. The resulting pore systems contain micropores (see supporting material), and although introducing Cu(II) into siliceous micropore systems from aqueous solutions is not straightforward [28], the highly dispersed Cu(II) species already present in the mesopores as the pore system is being destroyed by zinc silicate formation quite likely end up largely in the emerging micropores.

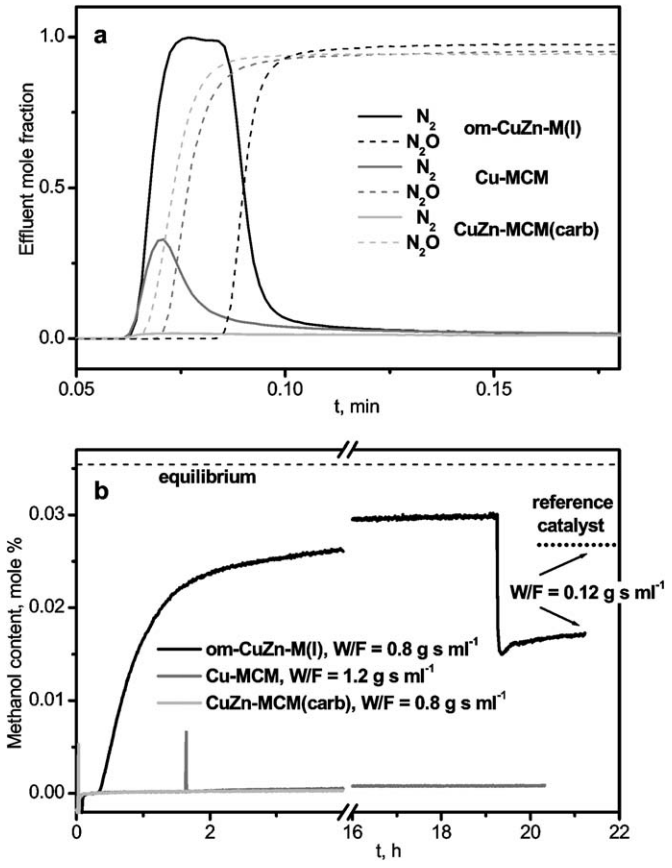

Fig. 5. N_2O frontal chromatography (a) and catalytic behavior in methanol synthesis at normal pressure ((b) $T = 493$, K; 72% H_2, 10% CO, 4% CO_2 and 14% He) measured with matrix-encapsulated Cu/ZnO catalysts.

3.3. Catalysis and Cu–ZnO interaction

Fig. 5 shows the first data on the catalytic behavior of the new materials in methanol synthesis (Fig. 5b) and relates to the accessible copper surface area (Fig. 5a). We present here rates measured under ambient pressure, even though data measured under realistic pressures might be more informative and less limited by equilibrium than data from ambient pressure tests. However, it is known that the results of such tests and of the much more laborious pressure tests are clearly correlated [37].

Table 2 summarizes the measured activities. Although differences between the samples could be expected based on the differing Cu contents and reduction behaviors, the contrast is striking. With om-CuZn–M(I), N_2O chemisorption yielded an appreciable Cu surface area, whereas the value measured with the monometallic Cu-MCM was surprisingly small and that of CuZn-MCM(carb) was near the detection limit. Analogously, only om-CuZn–M(I) provided an appreciable methanol synthesis activity, whereas the activities of the catalysts on the basis of MCM-48, which were measured at a higher W/F due to the very low methanol formation, were disappointingly low. With om-Cu–M(I), a gradual productivity increase with time on stream that extended over several hours was observed (Fig. 5b). The methanol mole fraction tended toward the equilibrium value, which was ca. 0.0354 mol% under our conditions as found in independent experiments with conventional $Cu/ZnO/Al_2O_3$ catalysts at high W/F. Indeed, with om-Cu–M(I), the methanol effluent concentration decreased only moderately on an almost seven-fold decrease in the W/F.

Table 2 also presents activity data measured with the commercial reference catalyst with the same (i.e., lower) W/F. Note, however, that here again the methanol yield is too close to equilibrium to allow a direct comparison of rates. To achieve such comparison at least on an approximate basis, the forward reaction rate ($r_{\rightarrow}$) was estimated from the measured one (r) by taking into account that $r = r_{\rightarrow}(1 - r_{\rightarrow}/r_{\leftarrow}) \approx r_{\rightarrow}(1 - Q/K_{eq}) \approx r_{\rightarrow}(1 - p_{CH_3OH}/p_{eq,CH_3OH})$, where $r_{\leftarrow}$ is the reverse reaction rate, K_{eq} is the equilibrium constant ($= (p_{CH_3OH}/p_{H_2}^2 p_{CO})_{eq}$) and Q is the corresponding ratio of actual partial pressures ($p_{CH_3OH}/p_{H_2}^2 p_{CO}$). The hydrogen and CO pressures cancel out each other, because they do not change at a methanol formation of 200–300 ppm. Forward reaction rates estimated on this basis are compared in the last columns of Table 2. From these data, it is clear that om-CuZn–M(I) indeed provides a methanol synthesis rate at the same order of magnitude as the commercial reference catalyst. When this methanol synthesis rate is related to the free copper surface area, the performance of the model catalyst om-CuZn–M(I) matches that of the reference catalyst. (The slight advantage of the former should not be overemphasized due to the considerable uncertainties inherent in the correction used.)

For the MCM-48-derived catalysts, only with the monometallic Cu-MCM was it possible to reliably measure the methanol content of the effluent; the data of CuZn-MCM(carb) (and of several other similar preparations) were near or beyond

Table 2
Active Cu surface area and methanol synthesis activities of Cu/ZnO in mesoporous matrices measured at different W/F at 493 K

Sample code	Cu surface area[a], A_{Cu} (m^2/g)	W/F (g s/ml)	Methanol formation rate			
			Measured data		Corrected for influence of equilibrium	
			Per g catalyst (μmol/(g h))	Per m^2 Cu surface (μmol/(m^2 h))	Per g catalyst (μmol/(g h))	Per m^2 Cu surface (μmol/(m^2 h))
Reference[b]	22.9	0.12	357	15.6	1424	62
om-CuZn–M(I)	5.3	0.8	61	11.5	387	73
		0.12	224	42	428	81
Cu-MCM	1.1	1.2	1.8	1.6		
CuZn-MCM(carb)	(0.4)	0.8	(0.6)	(1.5)		

[a] By N_2O frontal chromatography.
[b] Ca. 50% Cu, 35% ZnO, 15% Al_2O_3.

the detection limit. Despite the low activities observed, some conclusions can be drawn from these data. Thus, the promotional effect of the zinc may be assessed by comparing the ratio between the rates (per Cu surface area) of ZnO-promoted and monometallic Cu catalyst [at the higher W/F of (1 ± 0.2) g s/ml]. This ratio was ca. 45, again a rough estimate due to the high conversion achieved with om-CuZn–M(I) at $W/F = 0.8$. However, it allows one to conclude that the promotional effect of the zinc was absent in CuZn-MCM(carb): indeed, with a 30- to 40-fold increase of the rate/m^2 Cu over the unpromoted copper, a measurable methanol synthesis rate should have been expected even with the smaller Cu surface area of this catalyst.

It is remarkable that the catalysts based on the MCM-48 matrix did not meet expectations with respect to not only the catalytic activity, but also the Cu surface area. From the accessible Cu surface areas (Table 2), the size of the particles (assumed to be spherical) may be estimated as 12.7 nm for om-CuZn–M(I), 34 nm for Cu–M, and 76 nm for CuZn-MCM(carb)). This is far beyond the data derived from the EXAFS spectra after reduction at even higher temperatures (3 nm, 1.2–1.8 nm, and 3 nm, respectively). This huge discrepancy cannot be due to methodical uncertainty; particles tens of nm in size definitely would not be distinguishable from the reference spectrum of the Cu foil (see, however, Fig. 2). Wall effects may explain some of the difference, particularly in matrixes having suffered serious damage of the pore system, in which a large part of the Cu aggregates may be covered by the curved walls. In om-CuZn–M(I), contact with the ZnO nanoparticles will further decrease the accessible surface. We believe, however, that aggregation of small Cu crystallites into polycrystalline particles was a major contributor to the discrepancies observed. This effect should be most dramatic in narrow pores; when 2 or 3 particles grow from near points in a 2.5- to 3-nm pore system, the result may be an aggregate in which most of the surface of the individual particles ends up in boundaries with other particles and with the matrix walls.

In om-CuZn–M(I), all complications seen with the other type of preparation (i.e., interaction of zinc with the silica wall, structural damage in the pore system, blocking of the Cu surface by overly small pores, probably enhanced by piling up of metal particles) obviously were circumvented; there was accessible copper surface area, and the active copper sites were well promoted by the zinc oxide component. This new catalyst is remarkable in two aspects: Its catalytic activity is on the same order of magnitude as that of a commercial catalyst (particularly when related to the accessible surface area), and it opens up new opportunities for characterization of the Cu–ZnO interface.

Fig. 4 illustrates these opportunities for the study of Cu–ZnO_x interactions. Fig. 4a shows some Zn*K*-XAFS spectra obtained in preliminary studies on the reduction of such catalysts in CO-containing hydrogen. It can be seen that on treatment in 10% CO/H_2 at 695 K for 15 min, a new neighbor emerged between the first (Zn–O) and the second (Zn–Zn) scattering peaks. With om-CuZn–M(I), it is obvious that the neighboring (Zn–O, Zn–Zn) shells decreased at the same time. This is less clear for om-CuZn–M(II), but a comparison of structural models for the samples after reduction in CO/H_2 at 485 and 695 K (Table 3) gives the same result.

Table 3
Examples for fits of Zn*K* EXAFS spectra measured after the reduction of om-CuZn-M samples (cf. Figs. 4a and 4c)

T_{red}, gas	Atom	r (Å)	CN	σ^2 (10^3 Å^{-2})	E_0 (eV)
		om-CuZn–M(I)			
540 K, H_2[a]	O	1.97 ± 0.01	4.0 ± 0.2	4.8 ± 1.5	10.3 ± 2.4
	Zn	3.20 ± 0.02	5.9 ± 1.6	10.0 ± 2.8	-0.8 ± 2.3
695 K, CO/H_2[b]	O	1.97 ± 0.02	3.6 ± 0.6	5.0 ± 2.0	9.4 ± 1.8
	Cu	2.56 ± 0.02	1.8 ± 1.0	9.3 ± 5.7	-1.0 ± 3.0
	Zn	3.20 ± 0.02	3.7 ± 1.5	6.4 ± 3.2	-1.0 ± 3.0
	O	1.97 ± 0.02	3.5 ± 0.4	4.7 ± 2.3	9.7 ± 2.2
	Zn	2.55 ± 0.03	2.1 ± 1.6	10.5 ± 7.3	-1.0 ± 3.9
	Zn	3.20 ± 0.03	3.7 ± 1.8	6.2 ± 4.0	-1.0 ± 3.9
		om-CuZn–M(II)			
485 K, CO/H_2[b]	O	1.97 ± 0.02	3.1 ± 0.4	5.0 ± 2.6	8.5 ± 1.8
	Zn	3.16 ± 0.09	3.2 ± 3.9	17.3 ± 1.5	-9.5 ± 7.8
695 K, CO/H_2[b]	O	1.97 ± 0.02	2.8 ± 0.3	4.8 ± 2.2	10.3 ± 2.4
	Cu	2.51 ± 0.05	0.9 ± 0.9	6.8 ± 8.5	-6.0 ± 7.1
	Zn	3.19 ± 0.06	1.4 ± 1.7	9.3 ± 13.0	-6.0 ± 7.1
	O	1.96 ± 0.04	2.6 ± 0.8	4.1 ± 3.2	9.8 ± 3.8
	Zn	2.49 ± 0.08	1.1 ± 2.0	8.5 ± 14.1	-9.3 ± 13.2
	Zn	3.17 ± 0.08	0.9 ± 0.9	6.0 ± 8.3	-9.3 ± 13.2

[a] 5% H_2, He.
[b] 10% CO/H_2.

Based on current concepts of the metal–support interaction in Cu/ZnO catalysts, the new shell could arise from copper (Cu surface seen by ZnO_x migrating on the Cu surface or surface alloy). Alternatively, full reduction of defective ZnO nanoparticles, with or without assistance from adjacent Cu, might have resulted in Zn(0) nanoparticles, with the new neighbor being a (metallic) Zn shell. The models given in Table 3 and exemplified in Fig. 4c have been evaluated to address this question.

As to the states reduced at lower temperatures, a nanoparticulate ZnO phase can be clearly identified in om-CuZn–M(I) after 540 K, H_2. The Zn–Zn shell was where it was found in ZnO (3.21 Å [23]), but its CN was 6 instead of 12. In om-CuZn–M(II) after 485 K, CO/H_2, the Zn–Zn CN was further decreased to 3.2, and the Zn–Zn distance decreased. Indeed, the Zn–Zn signal was not at all pronounced in this case (Fig. 4a), due to a very large Debye–Waller factor reflecting mainly structural disorder at the low measurement temperature.

After reduction in CO/H_2 at 695 K, the new neighbor could be modeled as a Zn atom or a Cu atom, because these elements are difficult to distinguish in XAFS due to their slight difference in atomic number. With a Zn neighbor assumed, the Zn–Zn distance in what would be Zn metal nanoparticles became rather small in om-CuZn–M(II) (2.49 vs. 2.66 Å in the bulk metal). If ZnO were reduced, then a change in the XANES also might be expected, which was not the case. However, taken as ZnO reduction, the reduction degree achieved might be too small to cause measurable effects in the near-edge region. With a Cu

neighbor assumed, one may wonder about a rather high Cu–Zn CN of 1.8 in om-CuZn–M(I) and an unexpected trend: The sample om-CuZn–M(II) was prepared with low Zn content to force a higher percentage of ZnO_x into the Cu/ZnO interaction, which was not achieved. However, CNs are always subject to rather large uncertainties, particularly in multishell fits, and the smaller effect at low Zn content may indicate that part of the ZnO_x was still deactivated by interactions with the walls as in the aqueous preparations. This possibility is also supported by the EXAFS spectrum in Fig. 4a. Hence, although there are indications that the metal shell emerging on severe reduction is copper, an unambiguous interpretation requires further work. However, to our knowledge, Fig. 4 is the first XAFS demonstration of Zn redox properties in a catalyst with competitive methanol synthesis activity.

Because very high treatment temperatures were used for methanol synthesis catalysts, it is of particular importance to examine the Cu spectra of these samples, because significant sintering might be expected even with the short duration of thermal stress. Fig. 4b compares these spectra for treatments at 485–540 K (in H_2 or CO/H_2) and 695 K. With om-CuZn–M(I), the EXAFS remained virtually unchanged after the high-temperature treatment; that is, there was no growth of the primary particles. In om-CuZn–M(II), however, the intensity of the scattering events actually became smaller after high-temperature reduction. Because particle splitting is unlikely, this effect may be attributed to morphology changes (as discussed previously [1–3]) or to disorder effects. More work is needed to elaborate on these beginnings.

The measurements with CO_2-free syngas were made based on reports indicating that pretreatment of methanol synthesis catalysts in such a feed causes transient excess activity on exposure to the full (CO_2-containing) mixture, with subsequent decay to a stationary activity [8]. On the other hand, overreduction may lead to the formation of a (inactive) brass alloy on the surface [2]. The activity properties related to the spectra shown in Fig. 4 remain unknown, however. Work currently underway includes catalytic characterization of the catalysts far from equilibrium, optimization of the new catalyst type in terms of activity and suitability for studies of the Cu–ZnO interaction (also with IR spectroscopy), collection of a database for reliable interpretation of the XAFS spectra, and the attempt to correlate structural studies as presented in Fig. 4 with activity measurements.

4. Conclusion

A model methanol synthesis catalyst containing Cu and nanoparticulate ZnO in a mesoporous silica (average pore diameter, 5 nm) has been developed. In activity measurements at normal pressure, the methanol formation rate achieved by this catalyst was of the same order of magnitude as that provided by a reference catalyst of commercial significance, which had a fourfold-higher Cu surface area and a fivefold-higher Cu content. Thus, the methanol formation rates per m^2 of Cu were comparable for the commercial and model catalysts. The new catalyst was obtained by a sequence of thermal decomposition of a liquid heterocubane of Zn_4O_4 type $[CH_3ZnOCH_2CH_2OCH_3]_4$ in a mesoporous silica with wormhole-type pore system, followed by wet impregnation with copper nitrate. This method apparently avoids the problems encountered with various attempts to load MCM-48 with Cu and Zn using acetate solutions (i.e., interaction of zinc with the silica wall, leading to structural damage in the pore system, blocking of the Cu surface by overly small pores, probably enhanced by the piling up of small metal particles into polycrystalline aggregates), resulting in poorly accessible Cu surface areas and disappointing activities. The new model catalyst holds promise for use in investigation of the Cu–ZnO interaction. This has been demonstrated by Zn*K* EXAFS studies during the reduction in CO/H_2, which indicate significant changes in the zinc phase.

Acknowledgments

The work was funded by the German Science Foundation (DFG) in the framework of the Collaborative Research Center “Metal–Substrate Interactions in Heterogeneous Catalysis” (SFB 558), which is gratefully acknowledged. The authors thank Mrs. Susanne Buse for performing the TPR measurements and porosity analyses.

Supporting material

The online version of this article contains additional supplementary material.

Please visit DOI: 10.1016/j.jcat.2006.05.020.

References

[1] B.S. Clausen, J. Schiotz, L. Grabaek, C.V. Ovesen, K.W. Jacobsen, J.K. Norskov, H. Topsøe, Top. Catal. 1 (1994) 367.
[2] J.-D. Grunwaldt, A.M. Molenbroek, N.-Y. Topsøe, H. Topsøe, B.S. Clausen, J. Catal. 194 (2000) 452.
[3] P.L. Hansen, J.B. Wagner, S. Helveg, J.R. Rostrup-Nielsen, B.S. Clausen, H. Topsøe, Science 295 (2002) 2053.
[4] C.V. Ovesen, B.S. Clausen, J. Schiotz, P. Stoltze, H. Topsøe, J.K. Nørskov, J. Catal. 168 (1997) 133.
[5] M.M. Günter, T. Ressler, B. Bems, C. Büscher, T. Genger, O. Hinrichsen, M. Muhler, R. Schlögl, Catal. Lett. 71 (2001) 37.
[6] M.M. Günter, T. Ressler, R.E. Jentoft, B. Bems, J. Catal. 203 (2001) 133.
[7] N.-Y. Topsøe, H. Topsøe, J. Mol. Catal. A 141 (1999) 95.
[8] H. Wilmer, O. Hinrichsen, Catal. Lett. 82 (2002) 117.
[9] M. Kurtz, N. Bauer, C. Büscher, H. Wilmer, O. Hinrichsen, R. Becker, S. Rabe, K. Merz, M. Driess, R.A. Fischer, M. Muhler, Catal. Lett. 92 (2004) 49.
[10] I. Nakamura, T. Fujitani, T. Watanabe, T. Uchijima, J. Nakamura, Catal. Lett. 35 (1995) 297.
[11] I. Nakamura, T. Fujitani, T. Uchijima, J. Nakamura, J. Vac. Sci. Technol. A 14 (1996) 1464.
[12] J. Nakamura, I. Nakamura, T. Uchijima, Y. Kanai, T. Watanabe, M. Saito, T. Fujitani, Catal. Lett. 31 (1995) 325.
[13] W.P.A. Jansen, J. Beckers, J.C. Van der Heuvel, A.W.D. Van der Gon, A. Bliek, H.H. Brongersma, J. Catal. 210 (2002) 229.
[14] M. Bandyopadhyay, A. Birkner, M.W.E. van den Berg, K.V. Klementiev, W. Schmidt, W. Grünert, H. Gies, Chem. Mater. 17 (2005) 3820.
[15] M. Bandyopadhyay, M.W.E. van den Berg, W. Grünert, A. Birkner, W. Li, F. Schüth, H. Gies, Microporous Mesoporous Mater. 89 (2006) 158.

[16] S. Polarz, F. Neues, M.W.E. van den Berg, W. Grünert, L. Khodeir, J. Am. Chem. Soc. 127 (2005) 12028.
[17] O. Dag, I. Soten, S. Polarz, O. Celik, N. Coombs, G. Ozin, Adv. Funct. Mater. 13 (2002) 30.
[18] B.H. Han, S. Polarz, M. Antonietti, Chem. Mater. 13 (2001) 3915.
[19] L.M. Bronstein, S. Polarz, S. Smarsly, M. Antonietti, Adv. Mater. 13 (2001) 1333.
[20] V. Hornebecq, Y. Mastai, M. Antonietti, S. Polarz, Chem. Mater. 15 (2001) 3586.
[21] S. Polarz, Encyclopedia Nanosci. Nanotechnol. 6 (2004) 179.
[22] H. Gies, S. Grabowski, M. Bandyopadhyay, W. Grünert, O.P. Tkachenko, K.V. Klementiev, A. Birkner, Microporous Mesoporous Mater. 60 (2003) 31.
[23] O.P. Tkachenko, K.V. Klementiev, E. Löffler, I. Ritzkopf, F. Schüth, M. Bandyopadhyay, S. Grabowski, H. Gies, V. Hagen, M. Muhler, L. Lu, R.A. Fischer, W. Grünert, Phys. Chem. Chem. Phys. 5 (2003) 4325.
[24] R. Becker, H. Parala, F. Hipler, O.P. Tkachenko, K.V. Klementiev, W. Grünert, H. Wilmer, O. Hinrichsen, M. Muhler, A. Birkner, C. Wöll, S. Schäfer, R.A. Fischer, Angew. Chem. Int. Ed. 43 (2004) 2839.
[25] B. Smarsly, S. Polarz, M. Antonietti, J. Phys. Chem. B 105 (2001).
[26] S. Polarz, M. Antonietti, Chem. Commun. (2002) 2593.
[27] S. Polarz, F. Neues, M.W.E. van den Berg, W. Grünert, L. Khodeir, to be published.
[28] O.P. Tkachenko, K.V. Klementiev, M.W.E. van den Berg, N. Koc, M. Bandyopadhyay, A. Birkner, C. Wöll, H. Gies, W. Grünert, J. Phys. Chem. B 109 (2005) 20979.
[29] D.A.M. Monti, A. Baiker, J. Catal. 83 (1983) 323.
[30] F.W.H. Kampers, T.M.J. Maas, J. van Grondelle, D.C. Brinkgreve, D.C. Koningsberger, Rev. Sci. Instrum. 60 (1989) 2635.
[31] K.V. Klementiev, VIPER for Windows (Visual Processing in EXAFS Researches), freeware www.desy.de/~klmn/viper.html.
[32] A.L. Ankudinov, B. Ravel, J.J. Rehr, S.D. Conradson, Phys. Rev. B 58 (1998) 7565.
[33] O. Hinrichsen, T. Genger, M. Muhler, Chem. Eng. Technol. 11 (2000) 956.
[34] M. Borovski, J. Phys. IV 7 (1997) C2.
[35] O.P. Tkachenko, M.W.E. van den Berg, N. Koc, H. Wilmer, M. Muhler, W. Grünert, unpublished results.
[36] M. Mhamdi, E. Marceau, S. Khaddar-Zine, A. Ghorbel, M. Che, Y. Ben Taarit, F. Villain, Catal. Lett. 98 (2004) 135.
[37] H. Bielawa, M. Kurtz, T. Genger, O. Hinrichsen, Ind. Eng. Chem. Res. 40 (2001) 2793.